Plasmonics
https://doi.org/10.1007/s11468-019-01062-0

Strong Collectivity of Optical Transitions in Lead Halide Perovskite Quantum Dots

Junais Habeeb Mokkath[1]

Received: 1 September 2019 / Accepted: 1 November 2019

Abstract

Perovskite quantum dots (QDs) are attractive semiconducting materials for large-scale and low-cost optoelectronic devices owing to their size-tunable bandgap, high photoluminescence quantum yield, and outstanding charge transport. Comprehending/understanding their fundamental photo-physical properties is of significant applied importance. However, first-principles theoretical studies elucidating their optical features are relatively less explored. In this study, we investigate the optical characteristics of $CH3NH3PbX_3$ (X = I, Br, Cl) perovskite QDs having sizes below the Bohr exciton radius. We base our calculations on the linear combination of atomic orbitals (LCAO) real-time-propagation *rt*-TDDFT technique. Our results underline the strong collectivity in the optical excitations, ascertained using the decomposition weight of the electron-hole transition via transition contribution maps. We also demonstrate an appealing route to tune the optical excitations subject to an external electric field. The results presented in this work will contribute to enhancing our understanding of the optical properties of perovskite QDs.

Keywords TDDFT · Quantum dots · Strong collectivity

Introduction

Hybrid organic-inorganic halide perovskites, with the representative system methylammonium lead iodide ($CH3NH3PbI_3$), have shown surging research interest over the last few years as low-cost solution-processed materials with promising applications in photovoltaics [1–8], photocatalysis [9–11], light-emitting diodes [12–19], and thermoelectrics [20], to list a few. They feature the chemical formula of ABX_3, where A and B are monovalent and divalent cations, respectively, and X is a monovalent halide anion. The B cation (typically Pb or Sn), occupy the central site of an octahedron formed by six halide ions and a cation A, typically methylammonium (MA) or formamidinium (FA), located between the octahedra. Elements of the success of these materials can be associated with their flexibility in composition (different combinations of cations and anions) and morphology [21–24]. For instance, thin films of $CH3NH3PbX_3$ (X = Cl, Br, I) yield tunable emission spectra: Cl (410 nm) $\longrightarrow$ Br (530 nm) $\longrightarrow$ I (780 nm). The majority of the research on halide perovskites are focused on their bulk materials. However, recently, their low-dimensional forms such as quantum dots (QDs) has been synthesized [25–36]. QDs allow facile and scalable manufacturing with wide spectral tunability and yield strong prospects for applications in flexible displays, photovoltaics, lasers, and quantum computers [37–40]. Importantly, QDs yield spatial confinement of charge carriers [41, 42], enhancing the radiative recombination rates, which is the key advantage of QDs over films for optoelectronic applications. Despite a large amount of literature on the synthesis/fabrication of perovskite QDs, there is a limited number of first-principles theoretical studies elucidating their optical characteristics. Given the increasing variety of QDs, elucidating their optical properties via first-principles calculations is vital and contribute a step

Electronic supplementary material The online version of this article (https://doi.org/10.1007/s11468-019-01062-0) contains supplementary material, which is available to authorized users.

✉ Junais Habeeb Mokkath
j.mokath@kcst.edu.kw

[1] Department of Physics, Quantum Nanophotonics Simulations Lab, Kuwait College of Science And Technology, Doha Area, 7th Ring Road, P.O. Box 27235, Doha, Kuwait

towards tailor-made perovskite QDs with desired optical properties.

The light absorption properties of nano-objects such as QDs are highly sensitive to their geometry and the chemical composition, and can dramatically vary with respect to their bulk counterparts. From a theoretical perspective, this problem can be solved using a classical electrodynamics framework based on Maxwell's equations [43–48]. Despite the successful application of the abovementioned technique to elucidate the optical properties of a vast number of nano-objects, it is classical, and it cannot describe accurately the quantum mechanical effects such as fine-size effects [49–51], non-locality [52, 53] effects appearing in nano-objects smaller than approximately 10 nm. In fact, even quasi quantum mechanical techniques, such as the hydrodynamic model, may not be useful for quantitative predictions [54]. A way to solve this problem is to use a fully quantum mechanical framework such as the Time Dependent Density Functional Theory (TDDFT) [55–58]. It is a parameter-free framework (as far as the potential acting on the valence electrons is known) that will automatically take into account quantum mechanical effects as mentioned earlier directly and accurately. TDDFT has been implemented in both the frequency and time domain. TDDFT in the linear-response regime (lr-TDDFT) is often formulated in frequency space [59] in terms of the Casida matrix expressed in the Kohn-Sham electron-hole space [60–62]. The second method, the real-time-propagation formulation of TDDFT (rt-TDDFT) is based on integrating the time-dependent Kohn-Sham equations in time [63–65]. While lr-TDDFT is limited to the weak perturbation field to meet the requirement of the linear-response approximation, rt-TDDFT allows one to capture the effects of external fields both in the weak and strong interaction regimes [66, 67].

In this article, using the state-of-the-art rt-TDDFT calculations, we address some of the lingering fundamental questions about the nature of optical excitations in small perovskite QDs, in particular, optical modulations as a function of the composition and external electric field. To this aim, we modeled and simulated perovskite QDs with an average size of 1.40 nm and a total of 39 atoms. It is a widely acknowledged fact that in order for the structure to be considered a QD, its average size must be below 2 r_B, where r_B is the exciton Bohr radius. The Bohr radii for $MAPbBr_3$ and $MAPbI_3$, for instance, are 2.0 nm and 2.2 nm, respectively. Generally, the perovskite QDs explored have a diameter below 10 nm, with a general average size of 3.0 nm, and some of them even less than 1.8 nm [68–70]. We hope that the results of our theoretical study may contribute to the improvement of our understanding of the perovskite QDs optical properties that are of paramount importance for novel photovoltaic and photo-catalytic applications. The rest of this paper is organized as follows. First, we describe the systems we modeled and the simulations methods employed. We show our results and discuss them in the next section, addressing the absorption spectra and the transition contribution maps. The conclusions and outlook section closes the paper.

Model and Computational Aspects

All the results presented in this paper are obtained from the LCAO-rt-TDDFT technique [71–74] as implemented in the open-source real-space grid-based GPAW (version 1.40) software with the help of the atomic simulation environment (ASE) package [75]. This code is equipped with a number of post-processing tools [76] including the transition contribution map (TCM) [77], allowing the absorption spectrum to be decomposed into contributions from discrete electron-hole transitions with apparent relative weights [76, 77]. TCM is a useful visualization tool where a certain absorption peak arises from the superposition of multiple electron-hole transitions. Typically, the decomposition is represented as a two-dimensional plot with the energy of the unoccupied (occupied) given on the vertical (horizontal) axes of TCM. The distinct electron-hole transitions are indicated by spots on the TCM with an intensity proportional to the Kohn-Sham decomposition weight of the electron-hole transition [76]. The red (blue) illumination of the spots depicts the positive (negative) sign of the absorption decomposition of the electron-hole transition. More information regarding TCM plot can found in Ref. [76]. Besides, during the LCAO-rt-TDDFT simulations, the electron wavefunctions are evolved after a small external electric δ-pulse applied along the z-axis. The quantities of interest such as the time-dependent induced electron density, the time-dependent dipole moment, and the absorption spectrum can be determined. In the present work, we simulated the QD absorption spectrum with a Gaussian broadening of $\sigma = 0.10$ eV. We used a time step of 10 attoseconds and a total propagation time of 40 femtoseconds. We employed the B3LYP hybrid exchange-correlation functional [78], and the interaction between the ionic cores and the valence electrons are treated by the projector-augmented wave method (PAW) [79]. The pseudo wavefunctions are computed in real space with a grid spacing of 0.2 Å and the electron density and potentials are evaluated on a 0.15 Å grid. The QDs are surrounded by at least 10 Å of vacuum. We first subject the QDs to completely unconstrained structural optimization with the Broyden-Fletcher-Goldfarb-Shanno energy minimization algorithm as implemented in the ASE package. The minimization uses energies and forces calculated with DFT subjected to strict convergence conditions (SCF convergence: 10^{-8}, gradient convergence: 10^{-6}, and energy

convergence: 10^{-6}). Further, we incorporate the external electric field (up to ±0.20 V/m) to the Hamiltonian [73] to a representative cluster.

Results and Discussion

We start by analyzing the optical absorption spectra of $CH3NH3PbX_3$ (X = Cl, Br, I) QDs in Fig. 1. The first conclusion from these results is that, as we move from Cl ⟶ Br ⟶ I, the absorption onset blue-shifts systematically. We judge that it is a direct consequence of the increasing bandgap value, see the density of states (DOS) plots given in the right panel of Fig. 1. Furthermore, the calculated results are found to be in excellent qualitative agreement with the previous results on closely related fully inorganic $CsPbX_3$ (X = Cl, Br, I) perovskite QDs [27, 80]. Let us now proceed to analyze/discuss the absorption features of individual QDs separately starting from $CH3NH3PbCl_3$ QD. The absorption spectrum displays four clear features at 4.32 eV, 4.70 eV, 5.40 eV, and 6.45 eV. The peak at 5.40 eV shows the highest absorption intensity (total absorption value of 9.40 eV^{-1}) followed by the peak centered at 4.32 eV (total absorption value of 3.34 eV^{-1}). All the peaks as mentioned earlier are formed as a superposition of multiple electron-hole excitations. For example, the peak centered at 4.32 eV (5.40 eV) is composed of 13 (31) electron-hole excitations (see Supporting Information). Upon moving to $CH3NH3PbBr_3$ QD, one finds systematic variations in the absorption profile. In particular, absorption peaks blue-shifts at least 0.30 eV in comparison with the similar peaks of $CH3NH3PbCl_3$ QD. Also, one finds that $CH3NH3PbBr_3$ QD exhibits four absorption peaks at 4.60 eV, 5.0 eV, 5.72 eV, 6.80 eV in the absorption interval between 4.0 and 7.0 eV. The peak centered at 5.72 eV yields the highest absorption intensity (total absorption value of 9.81 eV^{-1}), and it is composed of 28 discrete electron-hole transitions (see Supporting Information). Dramatic spectral modulations emerge upon moving to $CH3NH3PbI_3$ QD, see Fig. 1. It is characterized by two pronounced/focused peaks centered at 4.93 eV (total absorption value of 10.11 eV^{-1}) and 6.09 eV (total absorption value of 10.24 eV^{-1}). These peaks are composed of 19 (20) discrete electron-hole transitions, see Supporting Information. The results shown in Fig. 1 manifest prominently that the intensity of the absorption peaks grows with the increasing size of the halide atoms: Cl ⟶ Br ⟶ I. The electronic structure via projected DOS (see right panel of Fig. 1) provides further information regarding the dominant states contributing to the absorption peaks. Note that the valence band maxima is dominated by the halide *p*-states, and the conduction band minima is formed by the overlap of the halide *p*-states and Pb *p*-states. This result is in good agreement with the previous theoretical [81] and experimental findings [27].

A detailed quantum mechanical insight into the main absorption peaks (obtained in Fig. 1) can be gained by inspecting the Kohn-Sham electron-hole transition contributions maps, see Fig. 2. This visualization tool is

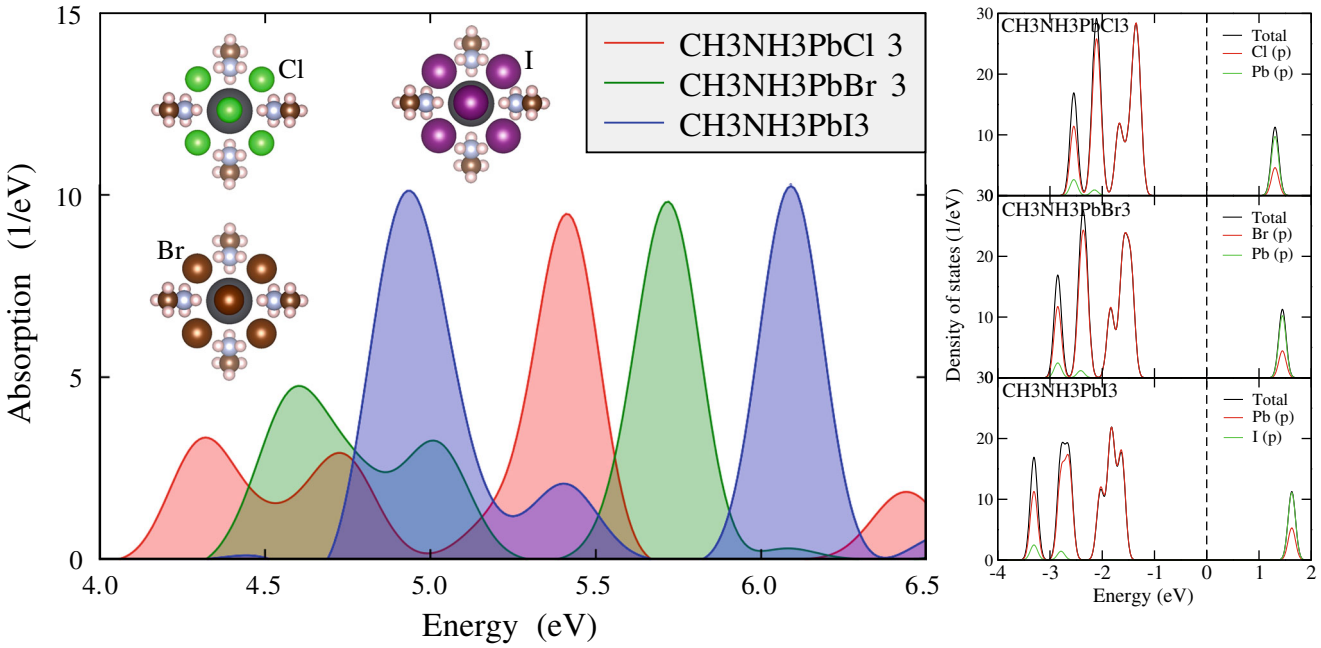

Fig. 1 Left: TDDFT calculated optical absorption spectra of $CH3NH3PbX_3$ (X = Cl, Br, I) QDs in the spectral range of 4.0 to 7.0 eV. Right: Electronic structure via density of states

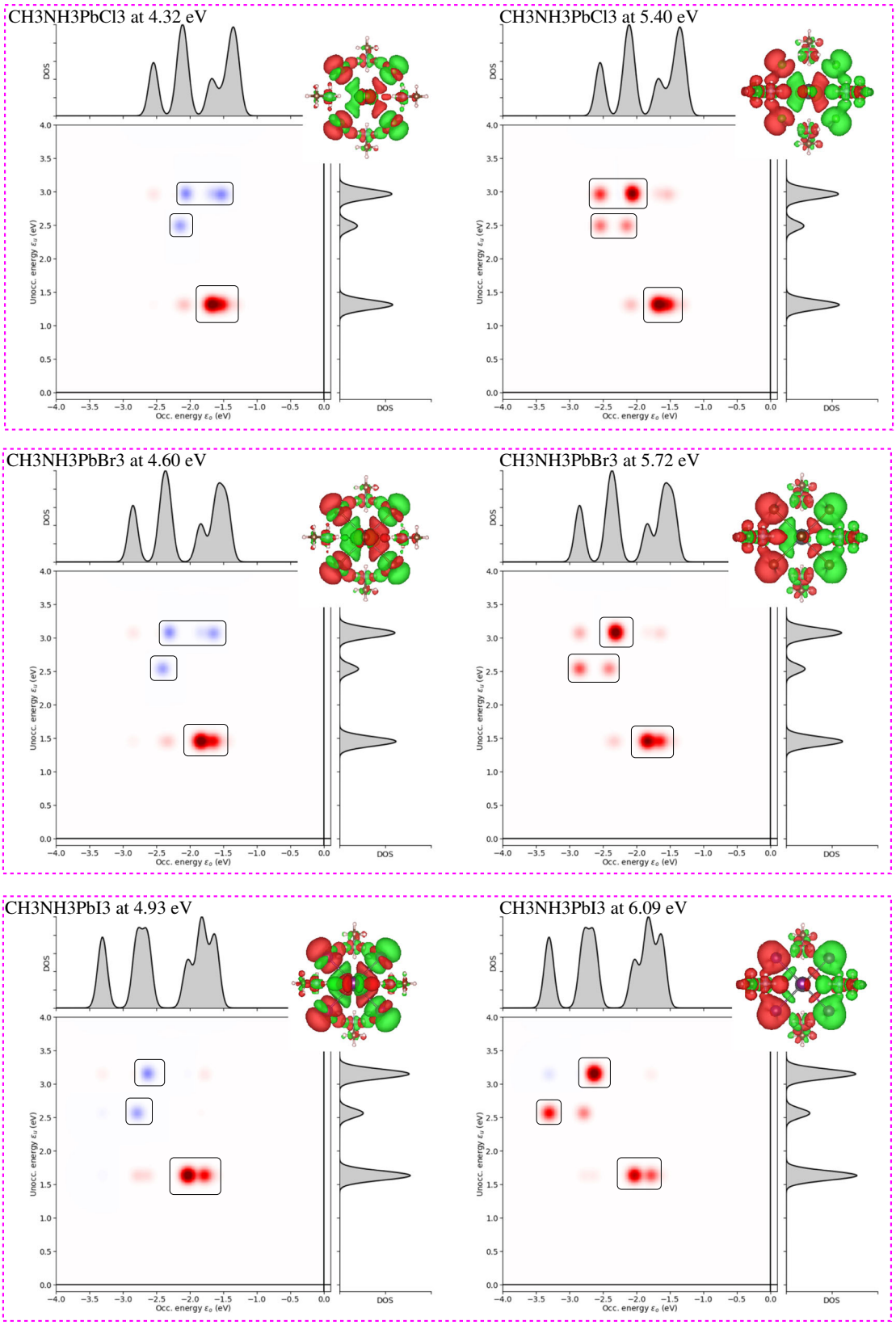

Fig. 2 Transition contribution maps for the photo-absorption decomposition of $CH3NH3PbX_3$ (X = Cl, Br, I) QDs at various energies. Red/blue illuminations denote positive/negative contribution to the transition. The brightness of the red/blue spots scales with the magnitude of contribution. The electron states are formed in the manifold of the initially unoccupied states, and the hole states are formed in the manifold of the initially occupied states

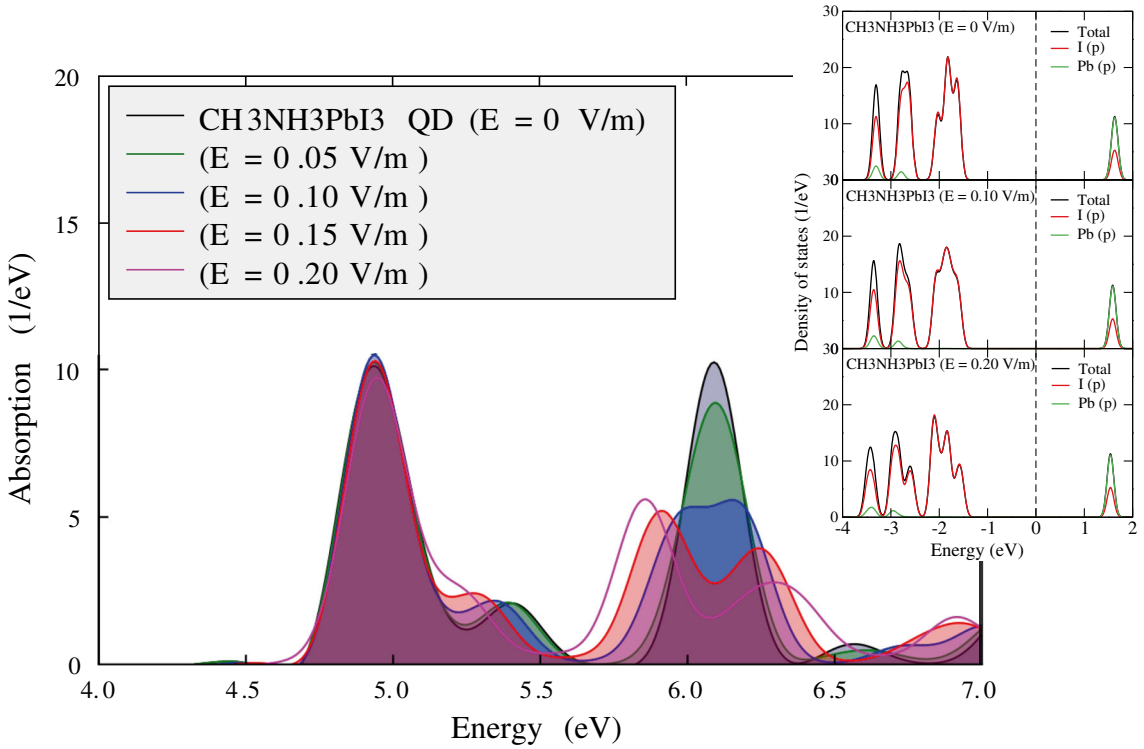

Fig. 3 Left: TDDFT calculated optical absorption spectra of $CH3NH3PbI_3$ QD as a function of the external electric field of 0.05 V/m, 0.10 V/m, 0.15 V/m, and 0.20 V/m. Right: Electronic structure via density of states

particularly useful when absorption peaks are formed due to the superpositions of several electron-hole transitions, and more importantly, it can be used in conjunction with TDDFT calculations. Besides, TCMs provide more useful insights which are not obtainable from local visualization methods such as transition densities [82] or natural transition orbitals [83]. In the TCM contours displayed in Fig. 2, the energies of the initial (occupied) and final (unoccupied) single-particle Kohn-Sham orbitals are shown in each sub-figure. Indeed, the induced charge density corresponding to the main peaks are also shown (on the right top panel of each sub-figure). Let us start analyzing the TCM plot of $CH3NH3PbCl_3$ QD corresponding to the peaks located at 4.32 eV and 5.40 eV. It highlights two major features. Firstly, there is a strong positive (constructive) contribution due to the contributions from the occupied

Table 1 Total absorption values of $CH3NH3PbI_3$ QD for 4.93 eV and 6.09 eV peaks for different electric field values

Applied electric field (V/m)	Total absorption values (1/eV)
E = 0.00	10.11 (4.93 eV) / 10.24 (6.09 eV)
E = 0.05	10.23 (4.93 eV) / 8.86 (6.09 eV)
E = 0.10	10.46 (4.93 eV) / 5.38 (6.09 eV)
E = 0.15	10.26 (4.93 eV) / 2.75 (6.09 eV)
E = 0.20	9.62 (4.93 eV) / 1.59 (6.09 eV)

p states into unoccupied states, see red spots in Fig. 2. Another prominent feature, particularly in the case of 4.32 eV peak is the appearance of the blue spots. Nevertheless, they emerge due to the negative contributions from occupied *d* states into unoccupied states (not shown in Fig. 2). Additionally, a visual inspection of the induced charge densities corresponding to the peaks at 4.32 eV and 5.40 eV reveals that the latter peak has strong collectivity (plasmon-like charge distribution) with respect to the former. Incidentally, this observation is in accordance with the number of discrete electron-hole transitions contributions: 4.32 eV (5.40 eV) peak is composed of 13 (31) transitions (see Supporting Information). After analyzing the TCM plots of $CH3NH3PbCl_3$ QD, we now proceed to analyze the TCM plots of $CH3NH3PbBr_3$ and $CH3NH3PbI_3$ QDs. Our visual inspection reveals a bunch of similarities and differences in comparison with the $CH3NH3PbCl_3$ TCM. An apparent similarity is that the first main peak of both the $CH3NH3PbBr_3$ (4.60 eV) and $CH3NH3PbI_3$ (4.93 eV) QDs show the red and blue spots, but in contrast, their second main peak shows red spots only. Additionally, the induced charge densities show more or less similar features. Indeed, as we move from Cl $\longrightarrow$ Br $\longrightarrow$ I, one observes clear differences in the location and intensity of the red and blue spots. In addition, the density of occupied states is seen to be red-shifts, and notable modification in the DOS peaks close to the Fermi level emerges, in contrast, as expected

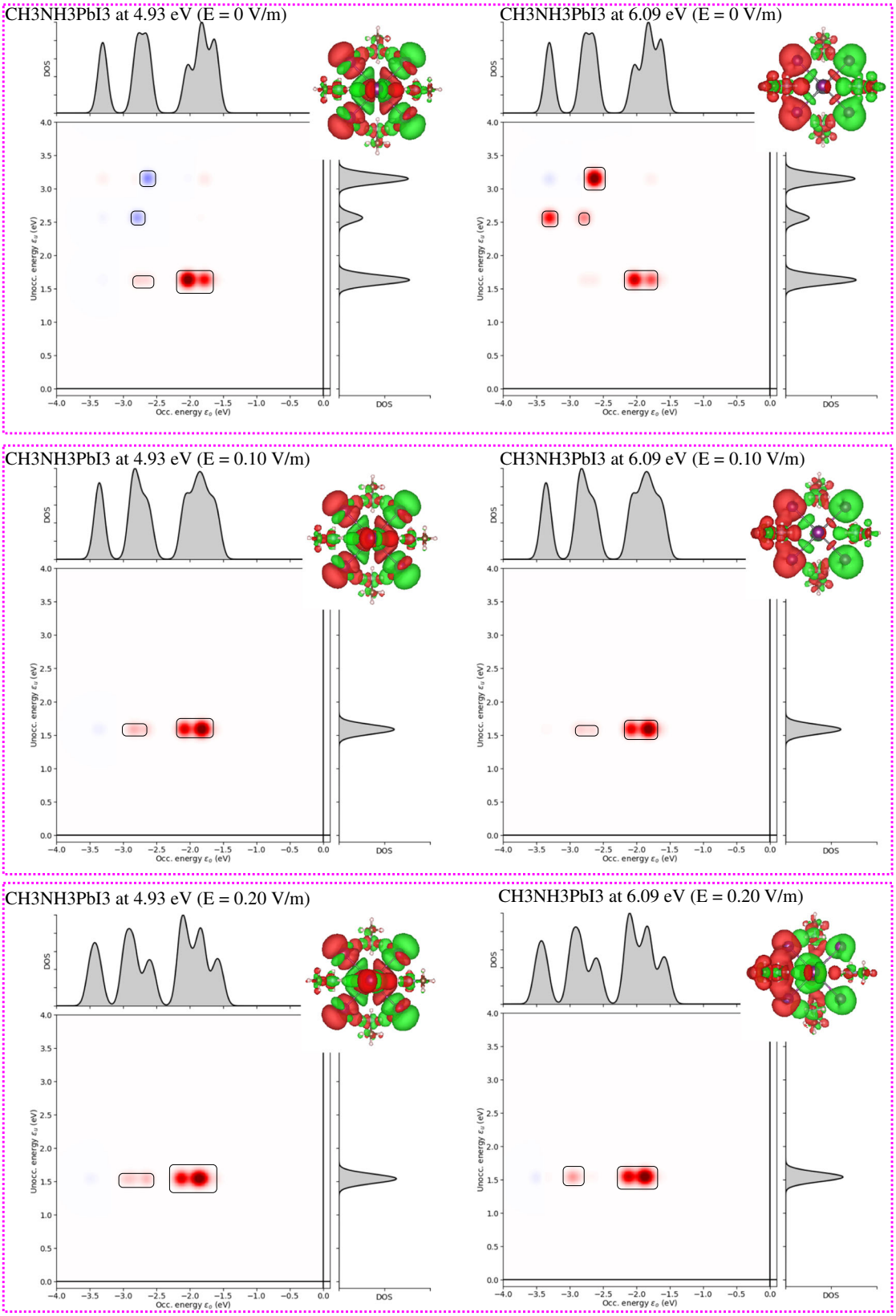

Fig. 4 Transition contribution maps for the photo-absorption decomposition of $CH3NH3PbI_3$ QDs at various energies as a function of the external electric field. Red/blue illuminations denote positive/negative contribution to the transition. The brightness of the red/blue spots scales with the magnitude of contribution. The electron states are formed in the manifold of the initially unoccupied states and the hole states are formed in the manifold of the initially occupied states

the density of unoccupied states remain unmodified. It should be emphasized that the main absorption peaks are dominated by many electron-hole transitions, and therefore, optical excitations with an increasing degree of spatial confinement. We speculate that the correlated motion of electrons and holes dominates the perovskite QDs response to optical excitation influencing its electrical and optical properties such as charge formation and mobility. Likewise, another important feature worth to mention is that most of the induced density is strongly confined on or near the surface of the QDs. Albeit, induced density also appears inside the QD. The coupling of the collective excitations to nearby electron-hole transitions also causes induced density oscillations inside the QDs [84].

Having cross-compared the optical features of $CH3NH3PbX_3$ (X = Cl, Br, I) QDs, we now turn our attention to tune the optical features through the inclusion of an external electric field (vary in the range of 0 to 0.20 V/m) in the Hamiltonian, see the results in Fig. 3. More specifically, we employed $CH3NH3PbI_3$ QD and applied external electric fields of 0.05 V/m, 0.10 V/m, 0.15 V/m, and 0.20 V/m. Apparently, the results shown in Fig. 3 portray that the key effect of incorporating an external electric field is to (slightly) modulate the characteristics of the first main peak at 4.93 eV and significant modifications of the second main peak at 6.09 eV and a substantial reduction of the total absorption value: see Table 1. For brevity, in the case of E = 0.05 V/m, there appears a minor reduction in the absorption intensity of 6.09 eV peak. However, the situation changes dramatically starting from E = 0.10 V/m. The total absorption value of the 6.09 eV peak has reduced to nearly half with respect to the spectrum without any electric field. Much more dramatic spectral

modulations (i.e., the second main peak transformed into a bimodal peak structure) emerges for the increasing value of the external electric field of E = 0.15 V/m and E = 0.20 V/m, see Fig. 3. Remarkably, the gross shape of the first dominant peak at 4.93 eV remains largely unaffected though a small reduction in the total absorption value is apparently visible: see Table 1.

The spectral modulations demonstrated in Fig. 3 can be traced back to the variations in the Iodine *p*-states, see DOS plots in the right panel of Fig. 3. The DOS plots establish that with the increasing value of the external electric field, the valance band edge states (composed of Iodine *p*-states) red-shift more or less systematically with substantial variations in the shape profile. Let us now focus our attention on TCM plots, see Fig. 4. For brevity, we show the TCM plots corresponding to the external electric field of 0.10 V/m, and 0.20 V/m along with the TCM without any electric field. One clearly observes that for E = 0.10 V/m and 0.20 V/m, only the red spots are visible and the *d* electron contributions (blue spots) more or less completely vanished. We also remark that by increasing the external electric field value, the number of electron-hole transitions contributing to the second main peak reduced significantly: see Supporting Information. As found previously, the induced density is mostly concentrated on or near the surface of the QDs. However, induced density also apparent inside the QD.

Concluding Remarks

In brief, we have presented a first-principles quantum mechanical study based on LCAO-*rt*-TDDFT technique elucidating the optical characteristics of $CH3NH3PbX_3$ (X = Cl, Br, I) QDs. Our results demonstrate that the strong collectivity in the QD optical excitations. As the main conclusion of our work, we show that the collectivity can be tuned subject to an external electric field. TCM technique combined with the visualization of the induced density provided a decent analysis of the collectivity of the dominant absorption peaks. This systematic analysis of the electron-hole contributions gives new insight into the optical excitations of perovskite QDs. It is our hope that the results obtained in this theoretical study would help in the rational design of perovskite QDs in optoelectronic devices.

Funding Information The research reported in this publication was supported by funding from Kuwait College of Science And Technology (KCST).

Supporting Information Available Total absorption values of $CH3NH3PbX_3$ (X = Cl, Br, I) QDs.

References

1. Kojima A, Teshima K, Shirai Y, Miyasaka T (2009) Organometal halide Perovskites as Visible-Light Sensitizers for photovoltaic cells. J Amer Chem Soc 131:6050. pMID: 19366264. https://doi.org/10.1021/ja809598r
2. Yang W, Noh JH, Jeon NJ, Kim YC, Ryu S, Seo J, Seok SI (2015) High-performance photovoltaic perovskite layers fabricated through intramolecular exchange. Science 348:1234. https://doi.org/10.1126/science.aaa9272, https://science.sciencemag.org/content/348/6240/1234.full.pdf
3. Im J-H, Lee C-R, Lee J-W, Park S-W, Park N-G (2011) 6.5% efficient perovskite quantum-dot-sensitized solar cell. Nanoscale 3:4088
4. Burschka J, Pellet N, Moon S-J, Humphry-Baker R, Gao P, Nazeeruddin MK, Grätzel M (2013) Sequential deposition as a route to high-performance perovskite-sensitized solar cells. Nature 499:316 EP
5. Wang R, Mujahid M, Duan Y, Wang Z-K, Xue J, Yang Y A review of perovskites solar cell stability. Adv Funct Mater 0:1808843. https://doi.org/10.1002/adfm.201808843
6. Jena AK, Kulkarni A, Miyasaka T (2019) halide Perovskite photovoltaics: background, status, and future prospects. Chem Rev 119:3036. https://doi.org/10.1021/acs.chemrev.8b00539

7. Grätzel M (2014) The light and shade of perovskite solar cells. Materials 13:838 EP
8. Zhou H, Chen Q, Li G, Luo S, Song T-B, Duan H-S, Hong Z, You J, Liu Y, Yang Y (2014) Interface engineering of highly efficient perovskite solar cells. Science 542:345. https://science.sciencemag.org/content/345/6196/542.full.pdf
9. Xu Y-F, Yang M-Z, Chen B-X, Wang X-D, Chen H-Y, Kuang D-B, Su C-Y (2017) CsPbBr3 perovskite quantum dot/graphene oxide composite for photocatalytic CO2 reduction. J Amer Chem Soc 139:5660. pMID: 28385017, https://doi.org/10.1021/jacs.7b00489
10. Wu W-B, Wong Y-C, Tan Z-K, Wu J (2018) Photo-induced thiol coupling and CH activation using nanocrystalline lead-halide perovskite catalysts. Catal Sci Technol 8:4257
11. Zhu X, Lin Y, Sun Y, Beard MC, Yan Y (2019) Lead-halide perovskites for photocatalytic-alkylation of aldehydes. J Amer Chem Soc 141:733. https://doi.org/10.1021/jacs.8b08720
12. Zhang Y, Guo T, Yang H, Bose R, Liu L, Yin J, Han Y, Bakr OM, Mohammed OF, Malko AV (2019a) Emergence of multiple fluorophores in individual cesium lead bromide nanocrystals. Nat Commun 10:2930
13. Tan Z.-K., Moghaddam RS, Lai ML, Docampo P, Higler R, Deschler F, Price M, Sadhanala A, Pazos LM, Credgington D, Hanusch F, Bein T, Snaith HJ, Friend RH (2014) Bright light-emitting diodes based on organometal halide perovskite. Nat Nanotechnol 9:687 EP
14. Cho H, Jeong S-H, Park M-H, Kim Y-H, Wolf C, Lee C-L, Heo JH, Sadhanala A, Myoung N, Yoo S, Im SH, Friend RH, Lee T-W (2015) Overcoming the electroluminescence efficiency limitations of perovskite light-emitting diodes. Science 350:1222. https://science.sciencemag.org/content/350/6265/1222.full.pdf
15. Shen Y, Cheng L-P, Li Y-Q, Li W, Chen J-D, Lee S-T, Tang J-X Pervskite light-emitting diodes: high-efficiency perovskite light-emitting diodes with synergetic outcoupling enhancement. Adv Mater 31:1970174. https://doi.org/10.1002/adma.201970174
16. Kumawat NK, Liu X-K, Kabra D, Gao F (2019) Blue perovskite light-emitting diodes: progress, challenges and future directions. Nanoscale 11:2109
17. Li G, Tan Z-K, Di D, Lai ML, Jiang L, Lim JH-W, Friend RH, Greenham NC (2015) Efficient light-emitting diodes based on nanocrystalline perovskite in a dielectric polymer matrix. Nano Lett 15:2640. pMID: 25710194, https://doi.org/10.1021/acs.nanolett.5b00235
18. Zhang L, Yang X, Jiang Q, Wang P, Yin Z, Zhang X, Tan H, Yang YM, Wei M, Sutherland BR, Sargent EH, You J (2017) Ultra-bright and highly efficient inorganic based perovskite light-emitting diodes. Nat Commun 8:15640 EP. article
19. Yuan M, Quan L, Comin R, Walters G, Sabatini R, Voznyy O, Hoogland S, Zhao Y, Beauregard E, Kanjanaboos P, Lu Z, Kim DH, Sargent EH (2016) Perovskite energy funnels for efficient light-emitting diodes. Nat Nanotechnol 11:872 EP. article
20. Wang M, Lin S Anisotropic and ultralow phonon thermal transport in organic inorganic hybrid perovskites: atomistic insights into solar cell thermal management and thermoelectric energy conversion efficiency. Adv Funct Mater 26:5297. https://doi.org/10.1002/adfm.201600284
21. Saparov B, Mitzi DB (2016) OrganicInorganic perovskites: structural versatility for functional materials design. Chem Rev 116:4558. pMID: 27040120, https://doi.org/10.1021/acs.chemrev.5b00715
22. Liao Y, Liu H, Zhou W, Yang D, Shang Y, Shi Z, Li B, Jiang X, Zhang L, Quan L, Quintero-Bermudez R, Sutherland BR, Mi Q, Sargent EH, Ning Z (2017) Highly oriented low-dimensional Tin halide perovskites with enhanced stability and photovoltaic performance. J Amer Chem Soc 139:6693. pMID: 28438016, https://doi.org/10.1021/jacs.7b01815
23. Li W, Wang Z, Deschler F, Gao S, Friend RH, Cheetham AK (2017) Chemically diverse and multifunctional hybrid organic-inorganic perovskites. Nat Rev Mater 2:16099 EP. review Article
24. Weidman MC, Seitz M, Stranks SD, Tisdale WA (2016) Highly tunable colloidal perovskite nanoplatelets through variable cation, metal, and halide composition. ACS Nano 10:7830. pMID: 27471862, https://doi.org/10.1021/acsnano.6b03496
25. Yao J-S, Ge J, Wang K-H, Zhang G, Zhu B-S, Chen C, Zhang Q, Luo Y, Yu S-H, Yao H-B (2019) Few-Nanometer-Sized CsPbI3 quantum dots enabled by strontium substitution and iodide passivation for efficient red-light emitting diodes. J Amer Chem Soc 141:2069. pMID: 30616341, https://doi.org/10.1021/jacs.8b11447
26. Gong X, Huang Z, Sabatini R, Tan C-S, Bappi G, Walters G, Proppe A, Saidaminov MI, Voznyy O, Kelley SO, Sargent EH (2019) Contactless measurements of photocarrier transport properties in perovskite single crystals. Nat Commun 10:1591
27. Protesescu L, Yakunin S, Bodnarchuk MI, Krieg F, Caputo R, Hendon CH, Yang RX, Walsh A, Kovalenko MV (2015) Nanocrystals of Cesium Lead Halide Perovskites (CsPbX3, X = Cl, Br, and I): novel optoelectronic materials showing bright emission with wide color gamut. Nano Lett 15:3692. pMID: 25633588, https://doi.org/10.1021/nl5048779
28. de Weerd C, Gomez L, Capretti A, Lebrun DM, Matsubara E, Lin J, Ashida M, Spoor FCM, Siebbeles LDA, Houtepen AJ, Suenaga K, Fujiwara Y, Gregorkiewicz T (2018) Efficient carrier multiplication in CsPbI3 perovskite nanocrystals. Nat Commun 9:4199
29. Zhang Q, Tavakoli MM, Gu L, Zhang D, Tang L, Gao Y, Guo J, Lin Y, Leung S-F, Poddar S, Fu Y, Fan Z (2019b) Efficient metal halide perovskite light-emitting diodes with significantly improved light extraction on nanophotonic substrates. Nat Commun 10:727
30. Chen Z, Turedi B, Alsalloum AY, Yang C, Zheng X, Gereige I, AlSaggaf A, Mohammed OF, Bakr OM (2019) Single-crystal MAPbI3 perovskite solar cells exceeding 21% power conversion efficiency. ACS Energy Lett 4:1258. https://doi.org/10.1021/acsenergylett.9b00847
31. Yin J, Yang H, Song K, El-Zohry AM, Han Y, Bakr OM, Brédas J-L, Mohammed OF (2018) Point defects and green emission in zero-dimensional perovskites. J Phys Chem Lett 9:5490. pMID: 30180582, https://doi.org/10.1021/acs.jpclett.8b02477
32. Byun J, Cho H, Wolf C, Jang M, Sadhanala A, Friend RH, Yang H, Lee T-W Efficient visible quasi-2D perovskite light-emitting diodes. Adv Mater 28:7515. https://doi.org/10.1002/adma.201601369
33. Yan F, Xing J, Xing G, Quan L, Tan ST, Zhao J, Su R, Zhang L, Chen S, Zhao Y, Huan A, Sargent EH, Xiong Q, Demir HV (2018) Highly efficient visible colloidal lead-halide perovskite nanocrystal light-emitting diodes. Nano Lett 18:3157. pMID: 29608317, https://doi.org/10.1021/acs.nanolett.8b00789
34. Kim Y-H, Wolf C, Kim Y-T, Cho H, Kwon W, Do S, Sadhanala A, Park C, Rhee S-W, Im SH, Friend RH, Lee T-W (2017) Highly efficient light-emitting diodes of colloidal metalHalide perovskite nanocrystals beyond quantum size. ACS Nano 11:6586. pMID: 28587467, https://doi.org/10.1021/acsnano.6b07617
35. Liu Y, Yang Z, Cui D, Ren X, Sun J, Liu X, Zhang J, Wei Q, Fan H, Yu F, Zhang X, Zhao C, Liu SF Two-inch-sized perovskite CH3NH3PbX3 (X = Cl, Br,I) crystals: growth and characterization. Adv Mater 27:5176. https://doi.org/10.1002/adma.201502597
36. Schmidt LC, Pertegás A, González-Carrero S, Malinkiewicz O, Agouram S, Mínguez Espallargas G, Bolink HJ, Galian RE, Pérez-Prieto J (2014) Nontemplate synthesis of CH3NH3PbBr3

perovskite nanoparticles. J Amer Chemi Soc 136:850. pMID: 24387158, https://doi.org/10.1021/ja4109209
37. Gong X, Yang Z, Walters G, Comin R, Ning Z, Beauregard E, Adinolfi V, Voznyy O, Sargent EH (2016) Highly efficient quantum dot near-infrared light-emitting diodes. Nat Photon 10:253 EP
38. Adachi MM, Fan F, Sellan DP, Hoogland S, Voznyy O, Houtepen AJ, Parrish KD, Kanjanaboos P, Malen JA, Sargent EH (2015) Microsecond-sustained lasing from colloidal quantum dot solids. Nat Commun 6:8694 EP. article
39. Xing J, Yan F, Zhao Y, Chen S, Yu H, Zhang Q, Zeng R, Demir HV, Sun X, Huan A, Xiong Q (2016) High-efficiency light-emitting diodes of organometal halide perovskite amorphous nanoparticles. ACS Nano 10:6623. pMID: 27284993, https://doi.org/10.1021/acsnano.6b01540
40. Utzat H, Sun W, Kaplan AEK, Krieg F, Ginterseder M, Spokoyny B, Klein ND, Shulenberger KE, Perkinson CF, Kovalenko MV, Bawendi MG (2019) Coherent single-photon emission from colloidal lead halide perovskite quantum dots. Science 363:1068. https://science.sciencemag.org/content/363/6431/1068.full.pdf
41. Kumar P, Muthu C, Nair VC, Narayan KS (2016) Quantum confinement effects in organic lead tribromide perovskite nanoparticles. J Phys Chem C 120:18333. https://doi.org/10.1021/acs.jpcc.6b06545
42. Lin K, Xing J, Quan L, de Arquer FPG, Gong X, Lu J, Xie L, Zhao W, Zhang D, Yan C, Li W, Liu X, Lu Y, Kirman J, Sargent EH, Xiong Q, Wei Z (2018) Perovskite light-emitting diodes with external quantum efficiency exceeding 20 per cent. Nature 562:245
43. Jin R, Cao Y, Mirkin CA, Kelly KL, Schatz GC, Zheng JG (2001) Photoinduced conversion of silver nanospheres to nanoprisms. Science 294:1901. https://science.sciencemag.org/content/294/5548/1901.full.pdf
44. Averitt RD, Sarkar D, Halas NJ (1997) Plasmon resonance shifts of Au-Coated Au2S nanoshells: insight into multicomponent nanoparticle growth. Phys Rev Lett 78:4217
45. Myroshnychenko V, Rodríguez-Fernández J, Pastoriza-Santos I, Funston AM, Novo C, Mulvaney P, Liz-Marzán LM, García de Abajo FJ (2008) Modelling the optical response of gold nanoparticles. Chem Soc Rev 37:1792
46. Aizpurua J, Hanarp P, Sutherland DS, Käll M, Bryant GW, García de Abajo FJ (2003) Optical properties of gold nanorings. Phys Rev Lett 90:057401
47. Hao F, Nehl CL, Hafner JH, Nordlander P (2007) Plasmon resonances of a gold nanostar. Nano Lett 7:729. pMID: 17279802, https://doi.org/10.1021/nl062969c
48. Hentschel M, Utikal T, Giessen H, Lippitz M (2012) Quantitative modeling of the third harmonic emission spectrum of plasmonic nanoantennas. Nano Lett 12:3778. pMID: 22686215, https://doi.org/10.1021/nl301686x
49. Halperin WP (1986) Quantum size effects in metal particles. Rev Mod Phys 58:533
50. Townsend E, Bryant GW (2012) Plasmonic properties of metallic nanoparticles: the effects of size quantization. Nano Lett 12:429. pMID: 22181554, https://doi.org/10.1021/nl2037613
51. Zhang P, Feist J, Rubio A, García-González P, García-Vidal FJ (2014) Ab initio nanoplasmonics: the impact of atomic structure. Phys Rev B 90:161407
52. García de Abajo FJ (2008) Nonlocal effects in the plasmons of strongly interacting nanoparticles, dimers, and waveguides. Jo Phys Chem C 112:17983. https://doi.org/10.1021/jp807345h
53. David C, García de Abajo FJ (2011) Spatial nonlocality in the optical response of metal nanoparticles. J Phys Chem C 115:19470. https://doi.org/10.1021/jp204261u
54. Esteban R, Borisov AG, Nordlander P, Aizpurua J (2012) Bridging quantum and classical plasmonics with a quantum-corrected model. Nat Commun 3:825 EP. article
55. Marques M, Gross E (2004) Time-dependent density functional theory. Annu Rev Phys Chem 55:427. pMID: 15117259, https://doi.org/10.1146/annurev.physchem.55.091602.094449
56. Stratmann RE, Scuseria GE, Frisch MJ (1998) An efficient implementation of time-dependent density-functional theory for the calculation of excitation energies of large molecules. J Chem Phys 109:8218. https://doi.org/10.1063/1.477483
57. Runge E, Gross EKU (1984) Density-functional theory for time-dependent systems. Phys Rev Lett 52:997
58. Calais J-L (1993) Density-functional theory of atoms and molecules. Int J Quantum Chem 47:101. https://doi.org/10.1002/qua.560470107
59. Hsu C-P, Hirata S, Head-Gordon M (2001) Excitation energies from time-dependent density functional theory for linear polyene oligomers: butadiene to decapentaene. J Phys Chem A 105:451. https://doi.org/10.1021/jp0024367
60. Hsu C-P, Casida ME (2009) Time-dependent density-functional theory for molecules and molecular solids. J Mol Struct: THEOCHEM 914:3. time-dependent density-functional theory for molecules and molecular solids
61. Hsu C-P, Walker B, Saitta AM, Gebauer R, Baroni S (2006) Efficient approach to time-dependent density-functional perturbation theory for optical spectroscopy. Phys Rev Lett 96:113001
62. Andrade X, Botti S, Marques MAL, Rubio A (2007) Time-dependent density functional theory scheme for efficient calculations of dynamic (hyper)polarizabilities. J Chem Phys 126:184106. https://doi.org/10.1063/1.2733666
63. Yabana K, Bertsch GF (1996) Time-dependent local-density approximation in real time. Phys Rev B 54:4484
64. Yabana K, Nakatsukasa T, Iwata J-I, Bertsch GF (1121) Real-time, real-space implementation of the linear response time-dependent density-functional theory. Physica Status Solidi (b) 243. https://doi.org/10.1002/pssb.200642005
65. Sander T, Kresse G (2017) Macroscopic dielectric function within time-dependent density functional theoryReal time evolution versus the Casida approach. J Chem Phys 146:064110. https://doi.org/10.1063/1.4975193
66. Tussupbayev S, Govind N, Lopata K, Cramer CJ (2015) Comparison of real-time and linear-response time-dependent density functional theories for molecular chromophores ranging from sparse to high densities of states. J Chem Theory Comput 11:1102. pMID: 26579760, https://doi.org/10.1021/ct500763y
67. Alejandro V, Pablo G-G, Johannes F, García-Vidal FJ, Angel R (2016) Quantum plasmonics: from jellium models to ab initio calculations. 5(409):3
68. Castaneda JA, Nagamine G., Yassitepe E, Bonato LG, Voznyy O, Hoogland S, Nogueira AF, Sargent EH, Cruz CHB, Padilha LA (2016) Efficient biexciton interaction in perovskite quantum dots under weak and strong confinement. ACS Nano 10:8603. pMID: 27574807, https://doi.org/10.1021/acsnano.6b03908
69. Peng L, Geng J, Ai L, Zhang Y, Xie R, Yang W (2016) Room temperature synthesis of ultra-small, near-unity single-sized lead halide perovskite quantum dots with wide color emission tunability, high color purity and high brightness. Nanotechnology 27:335604
70. Cha J-H, Han JH, Yin W, Park C, Park Y, Ahn TK, Cho JH, Jung D-Y (2017) Photoresponse of CsPbBr3 and Cs4PbBr6 perovskite single crystals. Jo Phys Chem Lett 8:565. pMID: 28067051, https://doi.org/10.1021/acs.jpclett.6b02763
71. Mortensen JJ, Hansen LB, Jacobsen KW (2005) Real-space grid implementation of the projector augmented wave method. Phys Rev B 71:035109

72. Enkovaara J, Rostgaard C, Mortensen JJ, Chen J, Dułak M, Ferrighi L, Gavnholt J, Glinsvad C, Haikola V, Hansen HA, Kristoffersen HH, Kuisma M, Larsen AH, Lehtovaara L, Ljungberg M, Lopez-Acevedo O, Moses PG, Ojanen J, Olsen T, Petzold V, Romero NA, Stausholm-Møller J, Strange M, Tritsaris GA, Vanin M, Walter M, Hammer B, Häkkinen H, Madsen GKH, Nieminen RM, Nørskov JK, Puska M, Rantala TT, Schiøtz J, Thygesen KS, Jacobsen KW (2010) Electronic structure calculations with GPAW: a real-space implementation of the projector augmented-wave method. J Phys: Condens Matter 22:253202
73. Walter M, Häkkinen H, Lehtovaara L, Puska M, Enkovaara J, Rostgaard C, Mortensen JJ (2008) Time-dependent density-functional theory in the projector augmented-wave method. J Chem Phys 128:244101. https://doi.org/10.1063/1.2943138
74. Larsen AH, Vanin M, Mortensen JJ, Thygesen KS, Jacobsen KW (2009) Localized atomic basis set in the projector augmented wave method. Phys Rev B 80:195112
75. Larsen AH, Mortensen JJ, Blomqvist J, Castelli IE, Christensen R, Dułak M, Friis J, Groves MN, Hammer B, Hargus C, Hermes ED, Jennings PC, Jensen PB, Kermode J, Kitchin JR, Kolsbjerg EL, Kubal J, Kaasbjerg K, Lysgaard S, Maronsson JB, Maxson T, Olsen T, Pastewka L, Peterson A, Rostgaard C, Schiøtz J, Schütt O, Strange M, Thygesen KS, Vegge T, Vilhelmsen L, Walter M, Zeng Z, Jacobsen KW (2017) The atomic simulation environmenta Python library for working with atoms. J Phys: Condens Matter 29:273002
76. Rossi TP, Kuisma M, Puska MJ, Nieminen RM, Erhart P (2017) KohnSham decomposition in real-time time-dependent density-functional theory: an efficient tool for analyzing plasmonic excitations. J Chem Theory Comput 13:4779. pMID: 28862851, https://doi.org/10.1021/acs.jctc.7b00589
77. He Y, Zeng T (2010) First-principles study and model of dielectric functions of silver nanoparticles. J Phys Chem C 114:18023. https://doi.org/10.1021/jp101598j
78. Becke AD (1993) A new mixing of HartreeFock and local density-functional theories. J Chem Phys 98:1372. https://doi.org/10.1063/1.464304
79. Blöchl PE (1994) Projector augmented-wave method. Phys Rev B 50:17953
80. Huang H, Polavarapu L, Sichert JA, Susha AS, Urban AS, Rogach AL (2016) Colloidal lead halide perovskite nanocrystals: synthesis, optical properties and applications. Npg Asia Mater 8:e328 EP. review
81. Koliogiorgos A, Garoufalis CS, Galanakis I, Baskoutas S (2018) Electronic and Optical Properties of Ultrasmall ABX3 (A = Cs, CH3NH3/B = Ge, Pb, Sn, Ca, Sr/X = Cl, Br, I) Perovskite Quantum Dots. ACS Omega 3:18917. https://doi.org/10.1021/acsomega.8b02525
82. Jespersen KG, Beenken WJD, Zaushitsyn Y, Yartsev A, Andersson M, Pullerits T, Sundström V (2004) The electronic states of polyfluorene copolymers with alternating donor-acceptor units. J Chem Phys 121:12613. https://doi.org/10.1063/1.1817873
83. Martin RL (2003) Natural transition orbitals. J Chem Phys 118:4775. https://doi.org/10.1063/1.1558471
84. Ma J, Wang Z, Wang L-W (2015) Interplay between plasmon and single-particle excitations in a metal nanocluster. Nat Commun 6:10107 EP. article